Journal of Molecular Structure 1147 (2017) 569–581

Contents lists available at ScienceDirect

Journal of Molecular Structure

journal homepage: http://www.elsevier.com/locate/molstruc

Spectroscopic (FT-IR,^{1}H and ^{13}C NMR) characterization and density functional theory calculations for *(Z)-5-(4-nitrobenzyliden)-3-N(2-ethoxyphenyl)-2-thioxo-thiazolidin-4-one (ARNO)*

K. Toubal [a], N. Boukabcha [b, *], Ö. Tamer [c], N. Benhalima [b], S. Altürk [c], D. Avcı [c], A. Chouaih [b], Y. Atalay [c], A. Djafri [a], F. Hamzaoui [d]

[a] Laboratory of Applied Organic Synthesis (LSOA), Department of Chemistry, Faculty of Sciences, University of Oran 1 Ahmed Ben Bella, 31000, Oran, Algeria
[b] Laboratory of Technology and Solid Proprieties (LTPS), Abdelhamid Ibn Badis University of Mostaganem, 27000, Mostaganem, Algeria
[c] Department of Physics, Faculty of Arts and Sciences, Sakarya University, 54187, Sakarya, Turkey
[d] LPFM Académie de Montpellier, France

ARTICLE INFO

Article history:
Received 12 January 2017
Received in revised form
20 June 2017
Accepted 21 June 2017
Available online 22 June 2017

Keywords:
FT-IR
UV–Vis
DFT
Nonlinear optic
Frontier molecular orbitals

ABSTRACT

In this work, the vibrational spectral analysis is carried out by using FTIR spectroscopy in the range 4000 –400 cm^{-1} *(Z)-5-(4-nitrobenzyliden)-3-N(2-ethoxyphenyl)-2-thioxo-thiazolidin-4-one (ARNO)* molecule. Theoretical calculations were performed by using density functional theory (DFT) method using 6-31G (d, p) and 6-311G (d, p) basis sets. The results of the calculations were applied to simulated spectra of the title compound, which show excellent agreement with observed spectra. The first order hyperpolarizability and related properties (μ and α) for ARNO were also calculated. Stability of the molecule has been analyzed by natural bond orbital (NBO) analysis. Mulliken population analysis on atomic charges of the title compound has been carried out by the same method and basis sets. Finally, molecular electrostatic potential (MEP) and HOMO-LUMO energy levels have been evaluated.

1. Introduction

Non-linear optical (NLO) effects arise from the interactions of electromagnetic fields in various media to produce new fields altered in phase, frequency, amplitude or other propagation characteristics from the incident fields [1]. NLO is at the forefront of current research because of its importance in providing the key functions of frequency shifting, optical modulation, optical switching, optical logic, and optical memory for the emerging technologies in areas such as telecommunications, signal processing, and optical interconnections [2–5]. Organic molecules that exhibit extended π conjugation, in particular, show enhanced second order NLO properties [6].

The structure of the title compound, ARNO, has been studied by single crystal X–ray spectroscopy [7]. To the best of our knowledge, the literature survey reveals that the results based on quantum chemical calculations and FT-IR spectral studies on the title compound have not been reported, before. Herein, we have reported a detailed interpretation of IR spectrum based on the experimental and theoretical results of the compound, which are acceptable and supportable to each other. We have also interpreted the calculated spectra in terms of potential energy distribution (PED). This study may reveal the molecule is not only finding its applications in biological and pharmaceutical importance but also finds its importance in NLO applications.

2. General remarks

2.1. Experimental details

FT-IR spectrum was recorded as KBr pellets on a JASCOFT/IR4200 Fourier transform infrared spectrometer and the reported

* Corresponding author.
E-mail address: n.boukabcha@gmail.com (N. Boukabcha).

http://dx.doi.org/10.1016/j.molstruc.2017.06.102
0022-2860/

wavenumbers are given in cm^{-1}. ^1H and ^{13}C NMR spectra in $CDCl_3$ solution were recorded on a Bruker AC250 instrument at 298 K. Chemical shifts are reported as δ (ppm) relative to TMS as internal standard [8].

2.2. Computational details

The density functional theory [9] with the three-parameter hybrid functional (B3) [10] for the exchange part and the Lee–Yang–Parr (LYP) correlation function [11], level ab initio calculations have been carried out in the present investigation, using 6–31G(d, p) and 6–311G(d, p) basis set with Gaussian 03 [12] program package. An empirical, uniform scaling factor of 0.950 and 0.960 for the same basis sets respectively was used to offset the systematic errors caused by basis set in completeness, neglect of electron correlation and vibrational anharmonicity. A detailed assignment of vibrational modes has been carried out on the basis of potential energy distribution (PED) analysis [13,14].

Natural bond orbital (NBO) calculations of ARNO were performed at the B3LYP/6-31G(d) level using the NBO 3.1 program [15] included in the Gaussian 03 package. The energy of the first excited has been calculated by TD-B3LYP method using 6–31G (d, p) and 6–311G (d, p) basis sets [16–19]. The polarizabilities and first order hyperpolarizabilities for ARNO are calculated using B3LYP method in conjunction with 6–31++G(d, p) and 6-311++G(d, p) basis sets, based on the finite-field approach [20–24]. In the present of an applied electric field, the energy of a system is the function of electric field. The first hyperpolarizability is a third rank tensor that can be described by $3 \times 3 \times 3$ matrix. The 27 components of 3D matrix can be reduced to 10 components due to the Kleinman symmetry [25].

The components of β are defined as the coefficients in the taylor series expansion of the energy in the external electric field. When the electric field is weak and homogenous, this expansion becomes.

$$E = E^0 - \mu_i F_i - \frac{1}{2}\alpha_{ij}F_iF_j - \frac{1}{6}\beta_{ijk}F_iF_jF_k - \frac{1}{24}\gamma_{ijkl}F_iF_jF_kF_l + \ldots \qquad (1)$$

where E^0 is the energy of the unperturbed molecules, F_i is the field at the origin μ_i, α_{ij}, β_{ijk} and γ_{ijkl} are the components of dipole moment, polarizability, first and second order hyperpolarizability, respectively.

3. Results and discussion

3.1. Crystal structure

ARNO compound, *(Z)-5-(4-nitrobenzyliden)-3-N(2-ethoxyphenyl)-2-thioxo-thiazolidin-4-one (ARNO)*, crystallizes in space group $P\bar{1}$. From the single crystal X-ray diffraction data [7], it is observed that the crystal belongs to triclinic system with the following cell dimensions a = 9.1289(19), b = 9.3717(7), c = 12.136(3) Å, α = 102.133, β = 90.99 and γ = 117.165 (°), V = 895.4(3) $Å^3$ and Z = 2. The bond lengths, bond angles and torsional angles obtained for the optimized molecular structure of ARNO calculated at the B3LYP/6-31G (d, p) and B3LYP/6-311G (d, p) levels are given in Table 1. It can be seen in Table 1, B3LYP/6-31G (d, p) and B3LYP/6-311G (d, p) levels give similar results for bond lengths to experimental ones [7]. These results indicate that the values calculated by B3LYP method are quite consistent with the experimental values. In Table 1, The C–C bond lengths of phenyl ring have been calculated at the range of 1.387–1.410 Å by using B3LYP/6-31G (d, p) level and 1.387–1.411 Å by using B3LYP/6-311G (d, p) level. These bond lengths have been reported to be found at the region of 1.378(4)-

Table 1
The experimental [7] and calculated geometric parameters of the title compound.

Bond Lengths (Å)	XRD [7]	B3LYP/6-31G(d,p)	B3LYP/6-311G(d,p)
S1–C10	1.753(3)	1.785	1.785
S1–C8	1.753(3)	1.761	1.762
S2–C10	1.626(3)	1.640	1.643
O1–N1	1.223(3)	1.230	1.231
O2–N1	1.227(4)	1.230	1.229
O3–C9	1.211(3)	1.212	1.213
O4–C16	1.364(3)	1.356	1.355
O4–C17	1.447(4)	1.432	1.419
N1–C3	1.473(4)	1.470	1.487
N2–C10	1.384(3)	1.378	1.377
N2–C9	1.398(4)	1.411	1.420
N2–C11	1.439(3)	1.437	1.435
C1–C2	1.383(4)	1.387	1.387
C1–C6	1.392(4)	1.410	1.412
C2–C3	1.382(4)	1.393	1.393
C3–C4	1.379(4)	1.393	1.395
C4–C5	1.394(4)	1.388	1.387
C5–C6	1.390(4)	1.411	1.411
C6–C7	1.472(4)	1.450	1.454
C7–C8	1.331(4)	1.352	1.352
C8–C9	1.494(4)	1.492	1.491
C11–C12	1.373(4)	1.388	1.389
C11–C16	1.404(4)	1.407	1.405
C12–C13	1.390(4)	1.395	1.395
C13–C14	1.378(5)	1.393	1.393
C14–C15	1.380(5)	1.396	1.395
C15–C16	1.399(4)	1.399	1.400
C17–C18	1.493(6)	1.717	1.720
Bond Angles (°)			
C10–S1–C8	93.12(13)	92.8	92.8
C16–O4–C17	118.0(2)	118.9	118.9
O1–N1–O2	124.2(3)	124.8	124.8
O1–N1–C3	118.3(3)	117.6	117.6
O2–N1–C3	117.5(3)	117.7	117.6
C10–N2–C9	117.1(2)	116.9	117.5
C10–N2–C11	122.1(2)	122.2	122.4
C9–N2–C11	120.8(2)	119.7	119.8
C2–C1–C6	121.4(3)	122.0	121.5
C3–C2–C1	118.6(3)	118.4	118.5
C2–C3–C4	122.1(3)	121.9	121.8
C2–C3–N1	119.6(3)	119.5	119.1
C4–C3–N1	118.3(3)	118.8	119.0
C3–C4–C5	118.0(3)	118.1	119.1
C6–C5–C4	121.6(3)	121.0	120.9
C5–C6–C1	118.2(3)	118.0	118.1
C5–C6–C7	123.1(3)	123.9	124.5
C1–C6–C7	118.7(3)	118.0	117.3
C8–C7–C6	128.8(3)	133.3	131.3
C7–C8–C9	121.8(3)	120.2	119.2
C7–C8–S1	128.5(2)	134.0	135.0
C9–C8–S1	109.47(19)	109.7	109.8
O3–C9–N2	122.8(3)	123.8	123.7
O3–C9–C8	127.2(3)	126.1	126.2
N2–C9–C8	110.0(2)	111.1	110.1
C16–C11–N2	117.7(2)	117.6	118.4
O4–C16–C15	125.7(3)	125.6	125.4
O4–C16–C11	115.9(2)	115.9	115.9
Torsion angle(°)			
C6–C1–C2–C3	−1.3(5)	−0.24	−0.18
C1–C2–C3–C4	0.4(5)	0.23	−0.03
C1–C2–C3–N1	−179.3(3)	−179.6	−179.9
O1–N1–C3–C2	−18.1(4)	−17.9	−16.9
O2–N1–C3–C2	161.5(3)	160.0	163.8
O1–N1–C3–C4	162.2(3)	164.6	165.6
O2–N1–C3–C4	−18.2(4)	−179.9	−179.9
C2–C1–C6–C5	1.3(5)	0.5	0.3
C4–C5–C6–C7	−179.8(3)	−179.9	−179.9
C5–C6–C7–C8	21.0(5)	03.49	04.65
C1–C6–C7–C8	159.7(3)	177.7	176.7
C10–N2–C9–O3	178.2(3)	−178.4	−178.3
C10–S1–C8–C7	−170.7(3)	−178.4	−179.5
C10–N2–C11–C12	−82.7(3)	−90.12	−91.02
C9–N2–C11–C12	99.2(3)	96.45	94.47
C10–N2–C11–C16	98.4(3)	99.32	90.13

Table 1 (*continued*)

Bond Lengths (Å)	XRD [7]	B3LYP/6-31G(d,p)	B3LYP/6-311G(d,p)
C9–N2–C11–C16	−79.7(3)	−82.21	−84.36
C17–O4–C16–C11	177.4(3)	−178.20	−179.22
C14–C15–C16–O4	178.1(3)	179.0	179.9

1.404(4) Å [7]. The thiophene ring C–S bond lengths have been reported at 1.753(3) Å [7], and these bond lengths have been calculated at the range of 1.785–1.761 Å by using B3LYP/6-31G(d, p) and 1.785–1.762 Å by using B3LYP/6-311G (d, p). The S2–C10 bond length reported to be 1.626(3) [7] has been calculated at 1.640 and 1.643 Å, showing the double bond character of this bond. The bond length of S–C single bond in the thiazole ring has been reported as 1.81 Å, while that of C=S double bond has been declared at 1.61 Å [10]. The carbonyl group C=O bond lengths observed at 1.211(3) Å [7] has been calculated as 1.212 and 1.213 Å by using B3LYP/6-31G(d, p) and B3LYP/6-311G (d, p) levels, respectively. As for the calculated bond angles of ARNO, both levels give similar result as consistent with experimentally reported results [7]. The thiazole ring C10–S1–C8 bond angle observed as 93.12(13) ° has been calculated as 92.8° by using both levels. The largest difference for the bond angles between the experimental [7] and calculated results has been obtained for C8–C7–C6 angle. This bond angle has been reported as 128.8(3) ° [7]. The corresponding values have been calculated as 133.3° and 131.3° by using B3LYP/6-31G (d, p) and B3LYP/6-311G (d, p) levels, respectively. The bond angle for C16–O4–C17 reported to be 118.0 (2) ° has been also calculated as 118.9° by using both levels.

The donor and acceptor moieties have been divided into two planar systems. The donor part restricted between N1 and N2 forms a planar structure, while the acceptor part found at the phenyl ring and substituted tail group forms another planar structure.

The torsion angle C6–C7–C8–S1 has been calculated at-0.5167° and 1.643°, the C11–C16–O4–C17 torsion angle has been calculated at −179.22° and −179.56° by using B3LYP/6-31G (d, p) and B3LYP/6-311G (d, p) levels, respectively.

It can be also said that the computational levels used in this paper gives quite comparable results for bond lengths, bond angles and torsion angles for ARNO. The crystal structure and optimized geometry were presented in Fig. 1.

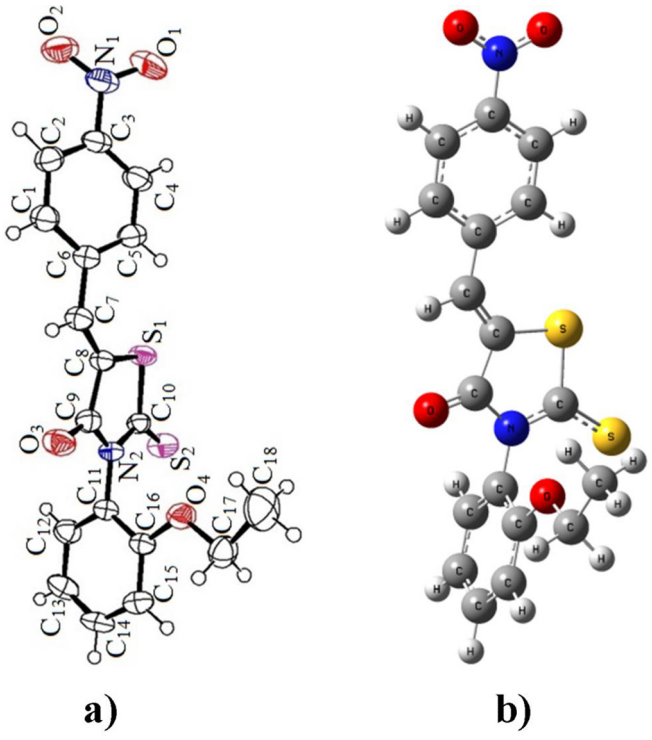

Fig. 1. **(a)** The experimental structure and **(b)** the theoretical structure using B3LYP/6-311G(d,p) method for ARNO.

3.2. Vibrational analysis

The ARNO molecule has 40 atoms and 114 normal vibrations from 3249 to 12 cm^{-1}, of which the strongest absorption mode is mode 84(1393 cm^{-1}, 474.7 kM/mol), and the weakest one is mode 4(44 cm^{-1}, 0.036 kM/mol). Based on optimized geometries, the vibrational frequencies have been calculated by the same method and basis. The assignments of vibrational bands have been made by using Gauss–View molecular visualization program, PED analysis and Silverstein et al. [24]. Theoretical and experimental [7] vibrational wavenumbers and the assignments of vibrational modes for the title compound are shown in Table 2.

3.2.1. NO_2 group vibrations

Aromatic nitro compounds have strong absorptions due to the asymmetric and symmetric stretching vibrations appeared in the range 1570–1485 and 1370–1320 cm^{-1} respectively [26]. In the present molecule, the strong bands at 1527 $cm^{-1}$by 6-31G** and 1525 cm^{-1} 6-31G** basis sets are assigned to asymmetric stretching mode of $NO_2$and the band at 1324 cm^{-1}assigned to symmetric stretching mode of NO_2. Aromatic nitro compounds have a band of weak–to–medium intensity in the region 590–500 cm^{-1} [27] due to the rocking deformation in plane mode of the NO_2 group. This vibration band was observed at 504 cm^{-1}. The deformation vibrations of NO2 group (wagging and twisting) contribute to several normal modes in the low frequency region [28]. These bands were also found in the wavenumber region around the characteristic position 749 cm^{-1} in FT–IR spectrum for ARNO.

3.2.2. Carbonyl group vibrations

It is well known that the carbonyl group exhibits a strong absorption band due to C=O stretching vibration and is observed in the region 1850–1550 cm^{-1}. Because of its high intensity and relatively interference free region in which it occurs, this band is easy to recognize. Infrared spectra of ARNO molecule, consists of two major bands in carbonyl stretching region; infrared bands at 1717 cm^{-1}. The calculated carbonyl stretching frequencies are found very close to observed ones (see Table 2).

3.2.3. Methyl group vibrations

The methyl (CH_3) groups absorb infrared radiation near 2960 and 2870 cm^{-1}. In many cases, only one band in 2870–2850 cm^{-1} can be resolved when both CH_3 and CH_2 groups are present in the molecule [29]. In our present work, the calculated vibrations (mode nos. 105–102) by 6-31G (d, p) basis set are predicted in the range 2986–2907 cm^{-1}, and by 6-311G (d, p) basis set in the range 2993–2920 cm^{-1}. These vibrations are assigned as the C–H stretching vibration of methyl group which is in good agreement with our experimental work; the absorption band observed at 2978 cm^{-1} and 2884 cm^{-1} in FT-IR spectrum. In our present work, the calculated vibrations (mode nos. 90, 88, 86 and 85) by 6-31G (d, p) basis set are predicted in the range 1439–1339 cm^{-1}, and by 6-311G (d, p) basis set in the range 1443–1348 cm^{-1}.

Table 2
The observed (FT–IR) and calculated frequencies (cm^{-1}), IR intensity (km mol^{-1}) and probable assignments (characterized by PED) of ARNO.

No	FT–IR	B3LYP/6–31G(d,p)			B3LYP/6–311G(d,p)			Assignments with PED>10%
		Unscaled (cm^{-1})	Scaled (cm^{-1})	I_{IR}	Unscaled (cm^{-1})	Scaled (cm^{-1})	I_{IR}	
114		3249	3086	2.337	3228	3099	2.792	ν CH A (80)
113		3248	3086	0.825	3227	3098	1.392	ν CH A (79)
112		3231	3069	7.461	3212	3083	6.269	ν CH B (79)
111		3226	3064	4.408	3209	3080	3.451	ν CH A (77)
110		3219	3059	13.22	3202	3074	12.01	ν CH B (83)
109		3206	3045	11.34	3188	3060	11.28	ν CH B (81)
108		3201	3041	3.927	3184	3056	3.521	ν CH A (72)
107		3192	3032	4.695	3174	3047	4.252	ν CH B (80)
106	3033	3168	3010	1.096	3150	3024	1.091	ν CH (71)
105		3143	2986	18.63	3118	2993	21.61	ν_{as} CH_3 (66)
104	2978	3136	2979	23.35	3110	2986	26.80	ν_{as} CH_3 (74)
103	2929	3061	2908	23.35	3047	2925	19.97	ν_{as} CH_2 (58) + ν_{as} CH_3 (10)
102	2884	3060	2907	13.04	3041	2920	14.17	ν_s CH_3 (84)
101	2855	3018	2867	37.34	3007	2887	37.05	ν_s CH_2 (73)
100	1717	1809	1718	207.6	1793	1721	233.8	ν C═O (20) + δ N_2CC (8) + ν C8–C9 (8)
99	1649	1668	1585	108.1	1653	1587	93.23	ν CC A (19) + δ CCH A (14)+ δ CCC A (10)
98		1661	1578	45.88	1646	1580	42.56	ν CC B (23) + δCCH B (25)+ δCCC B (11)
97		1659	1576	90.94	1643	1578	93.98	ν CC A (15) + δ CCH A (17)
96		1643	1561	8.686	1629	1564	8.325	ν CC A (21) + δ CCH A (27)+ δ CCC A (10)
95		1642	1560	4.025	1629	1563	4.129	ν CC B (28) + δCCH B (30)+ δCCC B (13)
94	1597	1607	1527	94.97	1589	1525	137.3	ν_{as} NO_2 (14) + ν CC A (25) + δ CCH A (26) + δ CCC A (11)
93		1551	1473	66.60	1537	1476	65.28	ν CC B (11) + δCCH B (24)+ τ CH_2CH_3(22)
92		1535	1458	14.71	1526	1465	19.30	ν CC A (17) + δ CCH A (54)
91	1497	1532	1455	52.20	1520	1459	56.28	δCH2 (35) + δCCH B (13)
90	1480	1515	1439	7.907	1504	1443	8.098	δCH_3 (51) + τ $OCCH_3$(13)
89		1500	1425	26.53	1490	1430	27.93	ρCH B (36) + ν CC B (15)
88		1500	1425	6.590	1486	1427	8.842	δCH_3 (66) + τ $OCCH_3$(19)
87		1452	1379	15.58	1442	1385	14.26	δ CCH A (43) + ν CC A (17)
86		1440	1368	38.79	1430	1373	39.92	δCH_3 (33) + δCCH_3 (15)
85		1410	1339	7.108	1404	1348	3.050	δCH_3 (34)+ δCCH_3 (15)+ δCCH_2 (11)+ δ OCH_2 (10)
84	1394	1393	1324	474.7	1376	1321	258.1	ν_s NO_2 (20) + ν CN1 (11) + δ NO_2 (16)
83		1387	1318	7.087	1374	1319	54.43	δ CCH A (15) + ν CC A (27) + δCCH (9)+ δC = CH (9)
82	1341	1380	1311	368.9	1368	1313	530.1	δCCH B (12) + ν CN2 (10) + ν CBN2 (7)
81		1357	1289	30.59	1349	1295	27.37	ρ CH A (33) + ν CC A (15)
80		1355	1287	43.11	1336	1282	47.65	δCCH B (18) + ν CC B (35)
79		1329	1262	11.86	1324	1271	18.85	ρ CH A (46) + ν CC A (10)
78	1286	1321	1255	114.1	1312	1260	80.87	ρCH B (36)+ ν CO (7)
77		1309	1243	0.764	1307	1255	1.052	τ CH_2CH_3(27) + τ $COCH_2$(10) + δ OCH_2 (15) + δCCH_2 (18)
76	1237	1300	1235	429.2	1288	1236	458.7	δCCH B (12) + ν CN_2 (9)
75		1282	1218	463.0	1270	1219	470.6	δCCH B (13)
74		1253	1190	8.693	1245	1196	8.390	δ CCH A (16)
73	1157	1217	1156	0.970	1213	1164	0.859	ν CC A (13) + δ CCH A (56)
72		1193	1133	20.52	1188	1141	14.88	ν CC B (11) + δCCH B (64)
71		1187	1128	12.63	1181	1134	5.016	τ CH_2CH_3(36) + δ OCH_2 (11)
70	1111	1186	1126	208.1	1176	1129	252.3	δCCH B (17)
69		1151	1093	51.24	1144	1098	50.98	CH_2CH_3(13) + δCCH B (15) + δCCH_3 (10)
68		1142	1085	3.857	1138	1092	6.172	δ CCH A (35)
67		1131	1075	50.07	1126	1081	50.55	δCCH B (14)
66		1130	1074	58.90	1121	1076	77.16	ν CC A (15)+ δ CCH A (25) + δ CCC A(12) + ν CN1 (8)
65		1075	1021	27.53	1068	1025	17.25	δCCH B (28) + ν CC B (16)
64	1034	1069	1016	41.47	1059	1017	65.16	δCCH B (14) + ν CC B (13) + δCCC B (11) ν CO (12) +ν CH_2–CH_3 (12)
63		1052	1000	12.85	1047	1005	10.28	τ CNCCB (11) + ν C═S (6) + ν CS (7) + δCCC B (12)
62		1047	995	74.93	1042	1001	83.14	δCCH B (8) + ν C8C9 (5)
61		1028	977	1.067	1028	987	0.786	ν CC A (18) + δCCH A (28) + δCCC A (34)
60		994	945	0.063	999	959	0.00	τ CH A (47) + τCCC A (13) + τN1CCH (12)
59		982	933	0.885	993	953	1.723	τCH B (36) + τ CH A (29)
58	921	982	933	0.872	987	948	0.074	τCH B (36) + τ CH A (29)
57		946	899	11.66	950	912	0.079	τCH B (24)
56		945	898	18.40	947	909	14.91	ω CH A (12) + τ CC═CH (10) + τ CCCH(17)
55	893	944	897	1.050	943	905	21.81	τCH B (49)
54		900	855	23.92	899	863	26.35	δCCH B (18)
53		867	824	21.06	872	837	44.17	ωCH B (33)
52	820	864	821	17.40	865	830	4.609	ω CH A (29) + τ C–CCHA(11)

Table 2 (*continued*)

No	FT–IR	B3LYP/6–31G(d,p)			B3LYP/6–311G(d,p)			Assignments with PED>10%
		Unscaled (cm^{-1})	Scaled (cm^{-1})	I_{IR}	Unscaled (cm^{-1})	Scaled (cm^{-1})	I_{IR}	
51		862	819	14.98	863	828	26.84	ωCH B (27)
50		837	795	1.478	840	806	1.016	ω CH A (49) + τ N1CCH (10)+ τ C–CCHA(13)
49		837	795	7.214	837	804	5.084	CH_2CH_3(17)+ ωCH B (17)
48		828	787	79.72	828	795	77.40	δCCH B (24)
47		800	760	20.37	797	765	16.56	δCCH B (22)
46		783	744	2.396	785	754	3.323	ωCH B (26)
45	749	763	725	20.45	763	733	49.54	ω CH A (21) + δCCC A (19) + ωNO_2 (10)
44		763	725	39.93	761	730	15.87	ωCH B (48) + δCCC B (10)
43		739	702	1.354	743	713	0.441	ω CH A (10)
42		723	687	2.436	730	701	2.520	ωCH B (20) + δCCC B (25)
41	679	698	663	20.71	702	674	25.38	omega; CH A (20) + δCCC A (24)
40		692	658	8.058	692	664	9.220	δCCC A (13) + δCCC B (11)
39		663	630	24.95	663	636	23.99	δCCC B (19) + δCCH B (14)
38		636	605	6.731	637	612	7.092	δ CCH A (20) + δCCC A (22)
37	586	616	585	16.11	616	591	17.41	τCCC B (19) + τCCH B (16)
36		600	570	37.68	601	577	43.26	τCCC B (17) + τCCH B (11)
35		585	556	1.025	587	564	1.710	τCH_2CH_3(15) + τCBNC = S(10)
34	540	558	531	4.122	561	538	2.961	τCH B (26) + τCCC B (21)
33		547	519	19.74	546	524	23.20	τCH B (18) + τCCC B (15)
32		534	507	5.477	533	510	1.394	ω CH A (19) + δCCC A (13)
31	504	531	505	1.068	529	508	10.21	ρ CH A (15) + δCCC A (12) + τρNO_2 (13)
30		511	486	0.084	509	489	0.378	τ CBNC=S(5)
29	428	483	459	2.565	483	464	4.549	τ CNCCB (10) + τCH B (26) + τCCC B (17)
28		447	424	0.832	442	424	1.349	ω CH A (15)+ δCCC A (14)
27		431	410	8.115	431	414	7.066	ν C–S (9)
26	398	417	396	0.385	415	399	0.313	τ CH A (22) + τCCC A (26)
25		411	390	10.31	409	393	9.701	δCCC A (15)
24		381	362	4.746	379	364	4.854	τ $OCCH_3$(5)
23		343	326	1.648	342	329	1.477	δCCCB(7)
22		335	318	4.002	334	321	3.839	δCCC B (11)
21		310	294	1.429	309	296	0.914	δCCCB(7)
20		306	290	0.684	303	291	0.531	τ C–CCCA(7)
19		294	279	1.156	293	282	1.132	τ CH_2CH_3(9)
18		263	250	0.399	261	251	0.390	τ CH_3(54) + τ $OCCH_3$(28)
17		240	228	4.591	241	231	4.608	τ CH_3(18) + τ$OCCH_3$(10)
16		193	184	1.821	192	185	1.567	δCCC B (11)
15		180	171	0.988	179	172	1.127	δCCC B (10)
14		173	165	0.745	172	165	0.664	τ N1CCC A (6)
13		171	162	0.277	169	162	0.169	τ N1CCC A (7)
12		160	152	0.357	159	153	0.306	τ N1CCC A (5)
11		111	105	0.451	107	103	0.475	τCH_3(19) + τ COCCB(26)
10		90	85	2.719	89	86	2.314	τ S=CNC(7)
9		80	76	0.943	79	76	0.608	τ CSC=C(5)
8		77	73	3.051	78	74	3.710	τ COCCB(10)
7		65	62	0.040	65	62	0.072	τNO2 (56)
6		64	61	0.189	58	55	0.131	τ CNCCB (17) + τ $COCH_2$(20) + τ COCCB(15) + τ COCC (10)
5		52	49	1.526	52	50	1.444	τ CNCCB (10)
4		44	42	0.036	44	42	0.049	τ CNCCB (11) + τ NCCCB (12)
3		21	20	0.123	24	23	0.167	τ CCCH(21) + τ C=C–CCA(23)
2		18	17	0.327	19	18	0.278	τ CNCCB (21) + τ C=C–CCA(11)
1		12	11	0.191	14	14	0.124	τ CNCCB (41)

ν: stretching; s, symmetric; as, asymmetric; ω: wagging; τ: twisting; δ: bending; ρ: rocking; vibrational modes are based on potential energy distribution (PED) and only contributions over 10% are given; unscaled and scaled frequencies are in unit of cm^{-1}; I_{IR} infrared inten. are in unit of km mol^{-1}; aromatic A: C9C11C13C14C16C18; aromatic B: C23C24C25C27C29C31.

These vibrations are assigned to CH3 deformation which show good agreement with our experimental work; the observed absorption band in FT–IR spectrum at 1480 cm^{-1}. The methyl torsion vibrations have a frequency range between 250 and 100 cm^{-1}. In our present work, the calculated vibrations (mode nos. 18, 17 and 11) by 6-31G (d, p) basis set are predicted in the range 250–105 cm^{-1}, and by 6-311G (d, p) basis set are predicted in the range 251–103 cm^{-1}. These vibrations are assigned to the out–of–plane bending vibration(torsion mode) of methyl group.

3.2.4. C–H vibrations

Aromatic compounds commonly exhibit multiple week bands in the region 3100–3000 cm^{-1} due to aromatic C–H stretching vibrations [30]. The bands appeared at 3086 to3032 cm^{-1} have been assigned to C–H ring stretching vibrations for ARNO. The C–H in–plane and out–of–plane bending vibrations generally lie in the range 1300–1000 cm^{-1} and 950–800 cm^{-1} [31,34], respectively. The C–H in–plane bending vibrations are identified at 1458, 1379, 1156, and 1133 cm^{-1} the observed absorption band in IR spectrum at 1157 cm^{-1}. Therocking C–H in–plane bending vibrations are identified at 1425, 1289 and1262 cm^{-1}. The waging C–H

Table 3
The experimental and calculated ^{1}H and ^{13}C NMR spectra for ARNO

	Chemical shifts		
	Experimental	6–31G(d,p)	6–311G(d,p)
^{1}H			
H_1	7.53	7.8925	7.7447
H_2	8.51	8.815	8.5813
H_4	8.53	8.9066	8.6931
H_5	7.53	8.0267	7.7142
H_7	7.79	7.8421	7.7000
H_{12}	7.50	7.4986	7.3238
H_{13}	7.40	7.4153	7.2507
H_{14}	7.45	7.833	7.6839
H_{15}	7.08	7.1497	6.9453
H_{17A}	4.11	4.2484	3.9062
H_{17B}	4.06	4.2484	3.9387
H_{18A}	1.42	1.782	1.5134
H_{18B}	1.40	1.716	1.4558
H_{18C}	1.38	1.3642	1.1712
^{13}C			
C1	128.35	128.288	141.204
C2	129.12	117.64	130.922
C3	147.96	141.007	155.434
C4	131.63	118.11	131.250
C5	121.00	121.938	134.919
C6	130.95	132.438	146.862
C7	123.26	123.189	135.276
C8	129.77	128.37	140.161
C9	167.19	158.982	174.495
C10	191.65	192.044	206.008
C11	131.63	118.556	132.988
C12	124.46	123.77	138.215
C13	113.48	112.866	126.349
C14	139.44	123.77	138.365
C15	113.48	104.596	115.627
C16	154.21	147.485	163.768
C17	64.43	60.3382	67.7673
C18	14.17	12.9652	17.1665

out–of–plane bending vibrations are identified at 824,821, 795, and 725 cm^{-1} the observed absorption band in FT–IR spectrum at 820 cm^{-1}. *C–N vibrations*.

Silverstein et al. [27] assigned C–N stretching absorption in the region 1382–1266 cm^{-1} for aromatic amines. In benzotrizole, the C–N stretching vibrations are found to be present at 1382 and 1307 cm^{-1} [31]. In the present study, a very strong band at 1341 cm^{-1}in FT-IR has been assigned to triazole C–N stretching vibration. The theoretically computed value of C–N stretching vibration is defined as 1311 cm^{-1}.

3.2.5. C–C vibrations

The C–C stretching vibration is in general appear in the spectral range 1650 to 1200 cm^{-1} [32–34]. The computed vibrations (mode 99) is assigned to C–C stretching vibration at 1585 cm^{-1} using B3LYP/6–311G (d, p) which is comparable to experimental data at 1649 cm^{-1}. The computed vibrations (modes 68, 65 and 61) are assigned to C–C–C in plane vibrations at 1085, 1021 and 977 cm^{-1} using B3LYP/6–31G (d, p). The computed vibrations (modes 37,34, 29 and 26) are assigned to C–C–C out of plane vibrations at 585, 531, 459 and 398 cm^{-1} using B3LYP/6–31G (d, p) which are comparable to experimental data at 586, 540, 428 and 398 cm^{-1}.

3.2.6. CH_2 group vibrations

The asymmetric C–H stretching mode of CH_2 group is expected in the region [35] around 2940 $cm^{-1}$and the symmetric around the region 2860 cm^{-1}. In ARNO the CH_2 asymmetric stretching mode is found at 2929 cm^{-1} in FT–IR spectra. The symmetric stretching modes also observed in FT–IR spectra at 2855 cm^{-1}. The calculated wave numbers of the above modes are 2908 cm^{-1} (58%) and cm^{-1} (73%) using B3LYP/6–31G (d, p) respectively for CH_2 asymmetric and symmetric stretching modes. The scissoring vibration of CH_2 were reported at 1609, 1575, 1560, 1542 cm^{-1} in FT-IR spectra [17,26]. The computed values of CH_2 give wave number at 1497 cm^{-1} by B3LYP/6–31G (d, p) method (mode no. 91).

3.3. ^{1}H and ^{13}C NMR spectra

In this study, relative chemical shifts were calculated by using the corresponding TMS shielding calculated at the same theoretical level and basis sets [36]. ^{1}H and ^{13}C chemical shifts for ARNO computed by B3LYP/6-31G(d, p) and B3LYP/6-311G(d, p) are listed in Table 3, as compared with previously reported experimental data. According to the comparison between experimental and calculated data, the calculated ^{1}H and ^{13}C chemical shifts are in acceptable agreement with the experimental results [8].

In this work, the peaks originated from the aromatic carbons have been calculated at the ranges of 104.596–147.485 by B3LYP/6–31G (d, p) and 115.627–163.768 ppm by B3LYP/6–311G (d, p) for ARNO molecule. The sulphur (S), nitrogen (N) and oxygen (O) atoms which have high electronegative property polarize the electron distribution in its bond to the adjacent carbon atom and decreases the electron density at the bridge for the title molecule. Therefore, C3, C9, C10 and C16 atoms give peaks at the downfield regions in NMR spectrum. The chemical shift values for the aliphatic C atoms observed as 64.43 and 14.17 ppm have been calculated as 67.7673 and 17.1665 ppm, respectively.

As for the ^{1}H NMR spectrum, a substantial agreements between the experimental [8] and theoretical results have been achieved for ARNO molecule. Aromatic proton signals observed at the range of 8.53–7.08 ppm have been calculated at the regions of 8.9066–7.1497 ppm by B3LYP/6-31G (d, p) and 8.6931–6.9453 ppm by B3LYP/6-311G (d, p). As would be expected, the aliphatic CH_2 and CH_3 protons give NMR signals to be moderately lower than aromatic ones.

3.4. Natural bond orbital analysis

NBO analysis provides an efficient method for studying intra–and inter–molecular bonding and interaction among bonds, and also provides a convenient basis for investigating charge transfer or conjugative interaction in molecular systems [37–40]. The second– order Fock–matrix was carried out to evaluate different types of donor–acceptor interactions and their stabilization energies in the NBO basis [41]. The interactions result in a loss of occupancy from the localized NBO of the idealized Lewis structure into an empty non–Lewis orbital. For each donor (i) and acceptor (j), the stabilization energy $E^{(2)}$ associated with the delocalization $(i \rightarrow j)$ is determined as

$$E^{(2)} = \Delta E_{ij} = q_i \frac{F^2_{(i,j)}}{\varepsilon_j - \varepsilon_i} \quad (2)$$

where q_i q is the donor orbital occupancy; $\varepsilon_j, \varepsilon_i$ are the diagonal elements and $F_{(i,j)}$ is the off diagonal NBO Fock matrix element.

Table 4
Second order perturbation theory analysis of fock matrix in NBO basis for ARNO.

Donor (i)	Type	ED (i) (e)	Acceptor (j)	Type	ED (j) (e)	$E^{(2)a}$ (kcal mol^{-1})	$(E_j-E_i)^b$ (a.u)	$F(i,j)^c$ (a.u)
N1–O1	π	1.98497	O2	LP(3)	1.44330	12.30	0.18	0.078
N1–O1	π	1.98497	N1–O1	π*	0.62920	7.42	0.32	0.052
C1–C6	π	1.58730	C2–C3	π*	0.38290	23.29	0.27	0.071
			C5–C4	π*	0.27619	17.35	0.28	0.064
			C7–C8	π*	0.21559	19.18	0.28	0.068
C2–C3	π	1.62963	N1–O1	π*	0.62920	27.56	0.15	0.061
			C1–C6	π*	0.37887	18.85	0.29	0.066
			C5–C4	π*	0.27619	20.00	0.29	0.070
C5–C4	π	1.65927	C1–C6	π*	0.37887	20.24	0.28	0.068
			C2–C3	π*	0.38290	19.68	0.28	0.067
C7–C8	π	1.83195	O3–C9	π*	0.27023	19.67	0.30	0.070
			C1–C6	π*	0.37887	11.36	0.31	0.056
C11–C12	π	1.71501	C13–C14	π*	0.33190	15.65	0.30	0.061
			C15–C16	π*	0.38363	21.71	0.29	0.072
C13–C14	π	1.67167	C11–C12	π*	0.36237	23.83	0.28	0.073
			C15–C16	π*	0.38363	17.34	0.27	0.062
C15–C16	π	1.64812	C11–C12	π*	0.36237	17.20	0.29	0.063
			C13–C14	π*	0.33190	22.55	0.29	0.073
S1	LP(2)	1.71876	S2–C10	π*	0.39355	31.79	0.18	0.070
			C7–C8	π*	0.21559	21.52	0.28	0.070
S2	LP(2)	1.85506	S1–C10	σ*	0.08559	13.62	0.36	0.063
			N2–C10	σ*	0.08449	13.40	0.61	0.082
N2	LP(1)	1.58888	S2–C10	π*	0.39355	70.71	0.20	0.106
			O3–C9	π*	0.27023	47.98	0.28	0.107
			C11–C16	σ*	0.03452	5.94	0.83	0.069
O2	LP(2)	1.89769	N1–O1	σ*	0.05672	19.23	0.71	0.105
			N1–C2	σ*	0.10466	12.68	0.57	0.076
O2	LP(3)	1.44330	N1–O1	π*	0.62920	164.02	0.14	0.139
O1	LP(2)	1.89765	N1–O2	σ*	0.05676	19.25	0.71	0.105
			N1–C3	σ*	0.10466	12.70	0.57	0.076
O3	LP(2)	1.83739	N2–C9	σ*	0.10525	31.08	0.65	0.129
			C8–C9	σ*	0.07950	21.33	0.66	0.108
O4	LP(1)	1.96216	C15–C16	σ*	0.02632	7.50	1.11	0.082
O4	LP(2)	1.83545	C15–C16	π*	0.38363	32.60	0.34	0.099

LP: lone pair.
[a] $E^{(2)}$ means energy of hyperconjugative interaction (stabilization energy).
[b] Energy difference between donor and acceptor i and j NBO orbitals.
[c] F(i, j) is the Fock matrix element between i and j NBO orbitals.

The larger the E(2) value, the more intensive is the interaction between electron donors and electron acceptors, i.e., the more the donating tendency from electron donors to electron acceptors, the greater the extent of conjugation of the whole system [42,43]. Delocalization of electron density between occupied Lewis-type (bond or lone pair) and formally unoccupied (antibond or Rydgberg) non–Lewis NBO orbitals correspond to a stabilizing donor-acceptor interaction. The intramolecular, rehybridization and delocalization of electron density (ED) within the title compound calculated by B3LYP/6-31G (d, p) methods are shown in Table 4. The stabilization energy E(2) associated with hyperconjugative interaction are shown in Table 4 which quantify the extend of intermolecular hydrogen bonding. The large E(2) value indicates the strong interaction between electron donors and electron acceptors. The strong intramolecular hyperconjugation interaction of the σ and π electrons of C–C to the anti C–C bond in the ring leads to stabilization of some part of the ring as evident from Table 4. For example, the intra molecular hyperconjugative interaction of π C2–C3 distribute to π* N1–O1, π* C1–C6 and π* C5–C4 leading to stabilization energy of 27.56, 18.85 and 20.00 kcal/mol. The another hyperconjugative interaction of LP(2) (S1) with σ* (S2–C10) leads to the stabilization energy of ~31.79 kJ/mol. The biggest hyperconjugative energy (164.02 kcal/mol) has been calculated for the interaction between LP(3) (O5) and σ* (N1–O1). The LP (1) N2 → π* (S2–C10) and LP (1) N4 → π* (O3–C9) interaction energies are 70.71 and 47.98 kcal/mol which clearly show the evidence for the elongation of the bond S2–C10 and O3–C9, respectively. These larger energies imply the hyperconjugation interaction between the electron donating groups to the acceptor.

The electron density (ED) at the conjugated π bonds (~1.59–1.66e) and π* bonds (~0.28–0.38e) of the aromatic benzene ring clearly showed that the strong delocalization leading to stabilization some part of the ring (C1–C6). The ED for the other ring

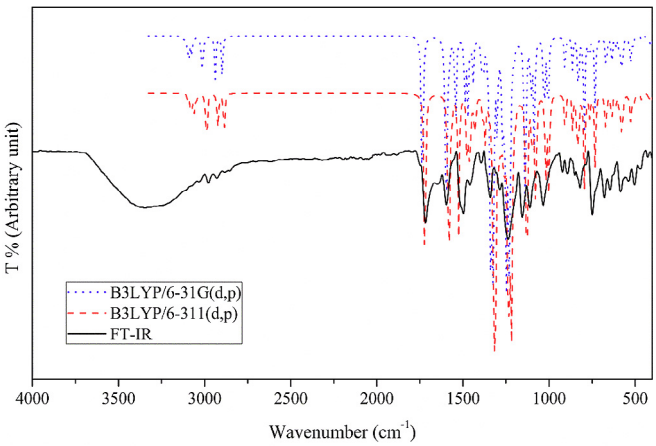

Fig. 2. Experimental and calculated IR spectra for ARNO.

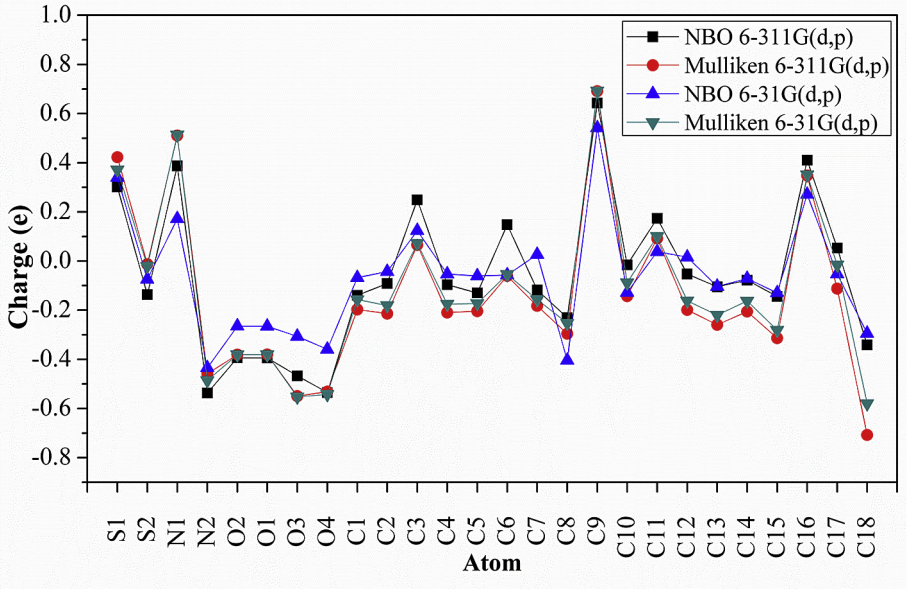

Fig. 3. Mulliken and NBO atomic charges for ARNO obtained by B3LYP level in conjunction with 6-31G(d,p) and 6-311G(d,p) basis sets.

(C11–C16) have been obtained at the range of ~1.65–1.72e for π bonds () and ~0.33–0.38e for π* bonds (see Fig. 2).

3.5. Atomic charge distributions

The reliable determination of the atomic charge populations is an important method for the investigation of several physico-chemical properties of molecular systems. Mulliken method [44] known as the oldest atomic charge analysis method is the cheapest and fastest way to obtain atomic charges. An important deficiency of Mulliken analysis is that the total charge is divided the canonical orbitals equally amongst the participating atoms without polarization effects. Another deficiency of Mulliken method is that it is very basis set dependent method. As for Natural bond orbital (NBO) analysis, it is known as a more reliable method since it considers the electron density and polarization effect. In NBO analysis, the localized natural atomic orbitals are used to describe the computed electron density [45]. The Mulliken and NBO atomic charges for the non-H atoms of ARNO calculated at the B3LYP using 6–31G (d, p) and 6–311G (d, p) levels are presented in Fig. 3. According to Fig. 3, Mulliken and NBO charge analysis methods give similar results to each other. The most positive charges has been found over carbonyl group C9 atom due to the bonding of electronegative O atom. Likewise, the N1 atom have large negative charge due to the coordination of O1 and O2 atoms. The methyl C atom (C18) has the biggest negative charge in ARNO molecule, since C18 is surrounded by the proton. The other negative charge centers can be calculated over the electronegative atoms such as N2, O3 and O4. All of the hydrogen atoms have been found to be carry positive charges, so these atoms have not been given in Fig. 3.

3.6. Non–linear optical effects

NLO effects arise from the interactions of electromagnetic fields in various media to produce new fields altered in phase, frequency, amplitude or other propagation characteristics from the incident fields. NLO is at the forefront of current research because of its importance in providing the key functions of frequency shifting, optical modulation, optical switching, optical logic, and optical memory for the emerging technologies in areas such as telecommunications, signal processing, and optical interconnections [46–49]. The non-linear optical response of an isolated molecule in an electric field $E_i(\omega)$ can be represented as a Taylor series expansion of the total dipole moment, μ_{tot}, induced by the field:

$$\mu_{tot} = \mu_0 + \alpha_{ij}E_j + \beta_{ijk}E_jE_k + \ldots \quad (3)$$

Where α_{ij} is the linear polarizability, μ_0 is the permanent dipole moment and β_{ijk} are the first hyperpolarizability tensor components. The isotropic (or average) linear polarizability is defined as [47]:

$$\alpha_{tot} = (\alpha_{xx} + \alpha_{yy} + \alpha_{zz})/3 \quad (4)$$

first hyperpolarizability is a third rank tensor that can be described by $3 \times 3 \times 3$ matrix. The 27 components of 3D matrix can be reduced to 10 components due to the Kleinman symmetry [50].

($\beta_{xyy} = \beta_{yxy} = \beta_{yyx} = \beta_{yzz} = \beta_{yzy} = \beta_{zyy}$; … Likewise other permutations also take same value). The output from Gaussian 09 provides 10 components of this matrix as.

Table 5
Calculated molecular dipole moment, polarizability and hyperpolarizability for ARNO.

Parameters	B3LYP/6–31G (d,p)	B3LYP/6–311G (d,p)
μ(D)	5.50	5.54
α (a.u)	295.93	307.23
$\alpha \times 10^{-24}$(esu)	43.9	45.5
β(a.u)	4292.04	4103.59
$\beta \times 10^{-30}$(esu)	37.08	35.45
$\beta \times 10^{-30}$(esu)	7.356 [52]	
$\beta \times 10^{-30}$(esu)	23.80 [53]	
$\beta \times 10^{-30}$(esu)	2.154 [54]	

β_{xxx} , β_{xxy} , β_{xyy} , β_{yyy} , β_{xxz} , β_{xyz} , β_{yyz} , β_{xzz} , β_{yzz} , β_{zzz} , respectively. The components of the first hyperpolarizability can be calculated using the following equation [51]:

$$\beta_i = \beta_{iii} + \frac{1}{3}\sum_{i\neq j}\left(\beta_{ijj} + \beta_{jij} + \beta_{jji}\right) \quad (5)$$

Using the x, y and z components of β, the magnitude of the first hyperpolarizability tensor can be calculated by:

$$\beta_{tot} = \left(\beta_x^2 + \beta_y^2 + \beta_z^2\right)^{1/2} \quad (6)$$

The complete equation for calculating the magnitude of β from Gaussian 03 output is given a follows:

$$\beta_{tot}\Big[= \left(\beta_{xxx}^2 + \beta_{xyy}^2 + \beta_{xzz}^2\right)^2 + \left(\beta_{xxy}^2 + \beta_{yyy}^2 + \beta_{yzz}^2\right)^2 + = \left(\beta_{xxz}^2 + \beta_{yyz}^2 + \beta_{zzz}^2\right)^2\Big]^{1/2} \quad (7)$$

The calculated values of the polarizabilities and the hyperpolarizabilities from Gaussian 03 output have been converted from atomic units (a.u) into electrostatic units (esu):(α: 1a.u. = 0.1482 × 10^{-24} esu; β: 1a.u. = 8.6393 × 10^{-33} esu). The electronic dipole moment (μ_i: i = x, y, z), the polarizability α_{ij} and the first hyperpolarizability β_{ijk} are shown in Table 5.

The total molecular dipole moment and first order hyperpolarizability are 5.4957 Debye and 37.08 × 10^{-30} esu obtained by B3LYP/6-31G (d, p), respectively and are depicted in Table 5.

The calculated polarizability α_{ij} have non zero values and was dominated by the diagonal components. Total polarizability (α_{tot}) calculated as 4.39 × 10^{-24} esu. The first hyperpolarizability value β of the title compound is equal to 35.45 × 10^{-30} esu obtained by B3LYP/6-311G (d, p). The hyperpolarizability β dominated by the longitudinal components of β_{xxx}. Domination of particular component indicates on a substantial delocalization of charges in this direction.

Organic π-systems with an electron donor (D) and an electron acceptor (A) represent an important class of the push–pull systems. D–A interaction, widely known as intramolecular charge-transfer (ICT), in such D–π–A molecules explain how the even more distinct optoelectronic properties occurs. From Fig. 4, the electron delocalization in ground state has been restricted between N1 and N2. In the first excited state, the electron delocalization has been found to be over the phenyl ring and substituted tail group. It can be said that the donor and acceptor moieties for ARNO are separated from each other. ICT from the ground state, HOMO (donor part), to the first excited state, LUMO (acceptor part), may be one of the reasons for considerable β parameter of ARNO. Another reason for considerable β parameter for ARNO is the extent of electron delocalization. It is well known that the extension of benzene derivatives has permitted an increase in the number of π electrons and their delocalization length, which lead to remarkable increase in the β value. As a consequence, the reason for high β parameter can be clearly explained by the above mentioned conditions (see Fig. 5).

The α and β parameters have been calculated as 43.9 × 10^{-24} esu and 37.08 × 10^{-30} esu by using B3LYP/6-31G (d, p) level, respectively. The same parameters have been obtained as 45.5 × 10^{-24} esu, 35.45 × 10^{-30} esu by using B3LYP/6-311G (d, p),respectively. Gobinath and Xavier [52] have calculated the β parameter for 3-methylbezothiazole-2-thione (3MBT2T) molecule by using B3LYP/6-311++G(d, p) level, and reported as 7.356 × 10^{-30} esu. In our previous study, the β parameter for 1-(4-chlorophenyl)-3-(4-chlorophenyl)-2-propen-1-one calculated by B3LYP/6-311++G (d, p) has been reported as 28.80 × 10^{-30} esu [53]. The same parameter for 3-methylbezothiazole-2-thione molecule has been calculated as 2.154 × 10^{-30} esu by using B3LYP/6-311++G (d, p) level [54]. When compared with the β parameter for ARNO with the similar compounds [52–54], it can be said that the ARNO has better nonlinear optical properties.

Table 6
Total energy (au), Dipole moment μ (D), Polarizability α × 10^{-23}(esu), First static hyperpolarizability β × 10^{-30}(esu) and HOMO–LUMO gap (eV) with the changing dihedral angle (C10–N2–C11–C16) for ARNO.

Φ	B3LYP/6-31G(d)				
	Energy	μ_{tot}	α_{tot}	β_{tot}	gap
00	−1900.95568	5.241	3.80	4.47	3.74
10	−1900.95702	5.260	3.82	4.34	3.72
20	−1900.95849	5.282	3.85	4.04	3.69
30	−1900.96097	5.319	3.88	3.64	3.65
40	−1900.96183	5.341	3.91	3.80	3.61
50	−1900.96383	5.385	3.95	4.95	3.56
60	−1900.96562	5.430	3.98	7.07	3.51
70	−1900.96789	5.482	4.02	9.82	3.47
80	−1900.96934	5.534	4.05	12.82	3.43
90	−1900.97053	5.585	4.08	15.79	3.39
100	−1900.97085	5.630	4.10	18.61	3.34
110	−1900.97131	5.671	4.13	21.25	3.31
120	−1900.97185	5.706	4.14	23.46	3.28
130	−1900.97204	5.729	4.16	25.28	3.26
140	−1900.97198	5.737	4.16	26.42	3.25
150	−1900.97206	5.735	4.17	27.25	3.25
160	−1900.95332	5.721	4.15	27.29	3.32
170	−1900.97249	5.699	4.16	26.98	3.25
180	−1900.97332	5.669	4.15	25.93	3.27

3.7. Frontier molecular orbitals (FMOs)

The highest occupied molecular orbitals (HOMOs) and the lowest–lying unoccupied molecular orbitals (LUMOs) are named as frontier molecular orbitals (FMOs). The FMOs play an important role in the optical and electric properties, as well as in quantum chemistry and UV–VIS spectra [55]. The HOMO represents the ability to donate an electron, LUMO as an electron acceptor represents the ability to obtain an electron. The energy gap between HOMO and LUMO determines the kinetic stability, chemical reactivity and optical polarizability and chemical hardness softness of a molecule [56]. The patterns of the HOMO and LUMO for the title compound calculated with the B3LYP/6-31G (d, p) level are given in Fig. 4. The positive phase is symbolized with red while the negative phase is symbolized with green. As can be seen that Fig. 4, HOMO and LUMO energies of the title compound are calculated as − 6.336512 and − 3.163904 eV for B3LYP/6–31G (d, p) level. The energy gaps between the HOMO and LUMO are calculated to be − 3.172608 eV.

The ARNO was investigated as a function of the twist angle and calculated the dipole moments (μ), polarizabilities (α) and hyperpolarizabilities (β), the twist angles ranging from 0 to 180°. The data for the title compound is shown in Table 4. The study shows that by changing the dihedral angle (C10–N2–C11–C16) should reduce the HOMO–LUMO energy gap for a particular dihedral angle allowing the molecular orbitals to overlap to have a proper electronic communication through conjugation. This is obvious when the frontier molecular orbital energies are studied using the GAUSSIAN 03. The variation of HOMO–LUMO energy

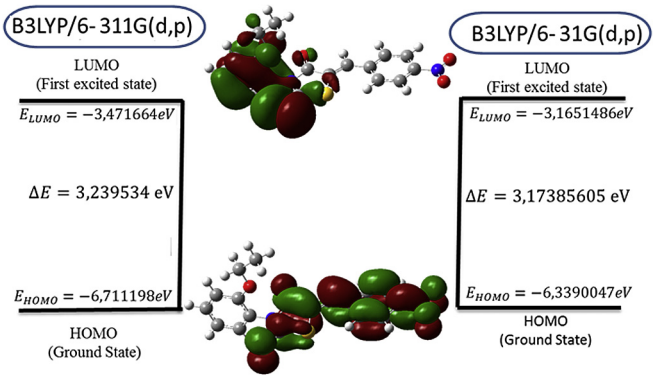

Fig. 4. The frontier molecular orbitals for ARNO obtained by B3LYP method.

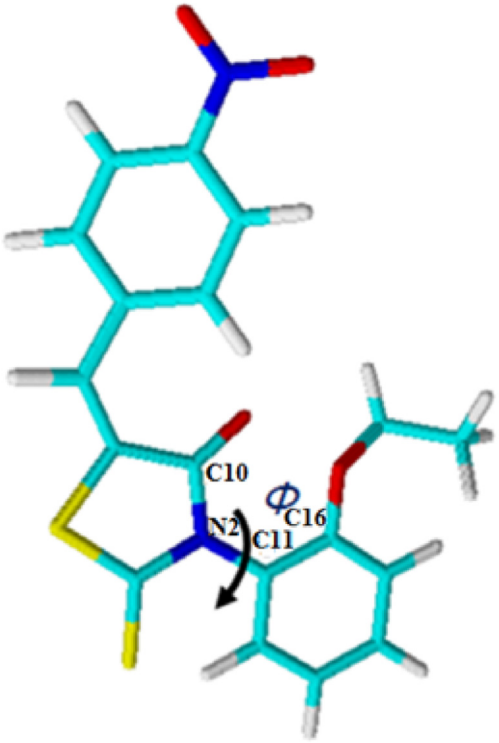

Fig. 5. The selected dihedral angle Φ **C10** –**N2**– **C11**– **C16** in ARNO.

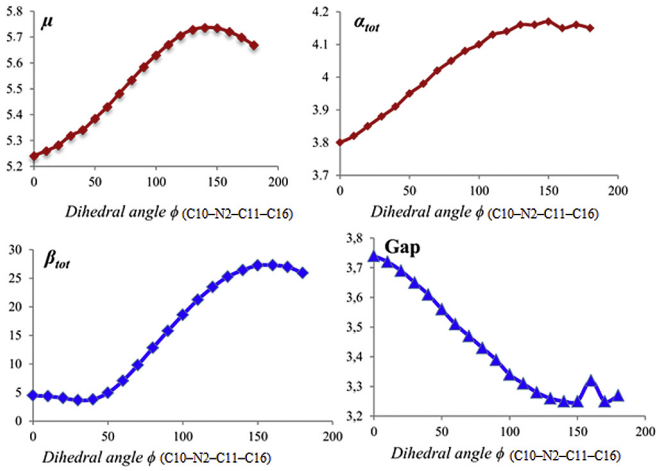

Fig. 6. The variation of linear and nonlinear optical properties with the changing dihedral angle for ARNO.

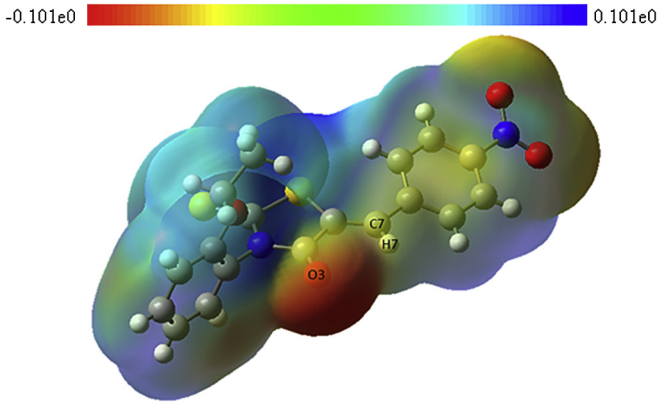

Fig. 7. Molecular electrostatic potential for ARNO.

gap with the dihedral angle for ARNO is given in Fig. 6. This will clearly show that the maximum hyperpolarizability is obtained for a non-planar structure. It is also seen that from Fig. 4 there is an inverse relationship between hyperpolarizability and the HOMO–LUMO gap.

3.8. Molecular electrostatic potential

The molecular electrostatic potential (MEP) is well–known as a rigorously defined expectation quantity which is measured as the first–order interaction between the molecular charge (electrons and nuclei) distribution and a positive unit charge at any point in space surrounding the molecule. An important feature of the electrostatic potential is that it is a real physical property that can be determined experimentally by diffraction methods, as well as computationally [54,58]. To predict reactive sites for electrophilic and nucleophilic attack for the investigated molecule, MEP was calculated at the B3LYP/6–31G (d, p) optimized geometry. The negative (red and yellow) regions of MEP were related to electrophilic reactivity and the positive (blue) ones to nucleophilic reactivity shown in Fig. 7. As a shown in Fig. 7, there are several possible sites for electrophilic attacks over the O5, O6, O7 and S2 atoms. The maximum negative electrostatic potential is substantially over the O7 atom because of the strong intermolecular hydrogen bond as can be seen from the MEP map of the title molecule, while regions having the negative potential are over the electronegative atoms, the regions having the positive potential are over the hydrogen atoms. Red and blue regions in the MEP map refer to the regions of negative and positive potentials and correspond to the electron rich and electron-poor regions, respectively, whereas the green color signifies the neutral electrostatic potential. The MEP surface provides necessary information about the reactivity of hard sites for the

Table 7
Thermodynamic parameters of ARNO calculated at B3LYP(6–31G(d, p)/6–311G(d, p))method.

T(K)	S(J/mol.K)		Cp(J/mol.K)		ΔH(kJ/mol)	
	6–31G(d,p)	6–311G(d,p)	6–31G(d,p)	6–311G(d,p)	6–31G(d,p)	6–311G(d,p)
100.00	454.03	451.04	170.32	169.72	11.02	10.98
200.00	604.60	600.77	277.47	275.49	33.36	33.19
298.15	735.62	730.83	385.44	382.76	65.91	65.51
300.00	738.01	733.21	387.42	384.74	66.63	66.22
400.00	863.46	857.88	486.83	484.17	110.48	109.80
500.00	981.20	975.05	568.38	565.99	163.39	162.46
600.00	1090.77	1084.21	633.00	630.91	223.59	222.43
700.00	1192.34	1185.49	684.31	682.48	289.55	288.19
800.00	1286.52	1279.43	725.65	724.02	360.12	358.59
900.00	1374.00	1366.73	759.45	757.99	434.43	432.75
1000.00	1455.51	1448.09	787.44	786.12	511.81	509.99

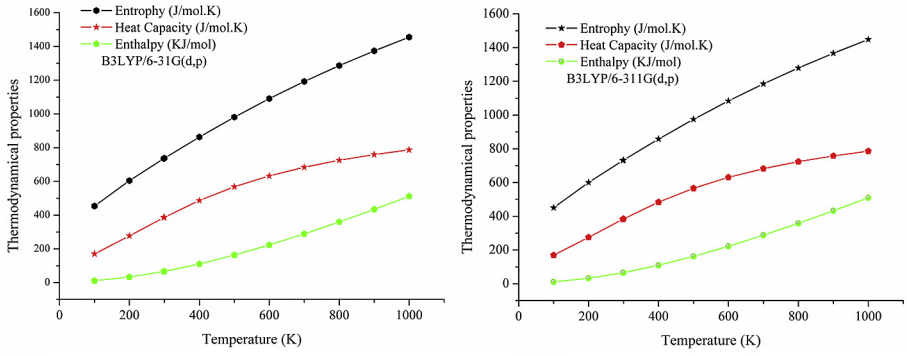

Fig. 8. Correlation graphic of entropy, heat capacity, enthalpy and temperature for ARNO.

investigated molecule (see Table 6).

3.9. Thermo-dynamical properties

The correlations between the statistical thermodynamics and temperature were also obtained. It is seen that the heat capacities, entropies and enthalpies increase when increasing temperature of a molecule and it also results that the intensity of the molecular vibrations increase with temperature. The standard statistical thermodynamic functions i, standard heat capacities, standard entropies and standard enthalpy changes (0→T) were obtained and are listed in Table 5. As can be seen from Table 7, the standard heat capacities, entropies and enthalpy changes increase at any temperature from 100.00 to 1000.00 K, since increasing the temperature causes an increase in the intensity of the molecular vibration. The correlation graphs are shown in Fig. 8. All the thermodynamic data supply helpful information for the further study on the ARNO. They can be used to compute the other thermodynamic energies according to relationships of thermodynamic functions and estimate directions of chemical reactions according to the second law of thermodynamics in thermo–chemical field [59].

4. Conclusion

This work presents the experimental and theoretical vibrational IR spectra of the title compound. All observed vibrational bands have been discussed and assigned on the basis on our DFT calculations. Scaled theoretical wavenumbers and PED results were quite useful for the reliable assignments of normal modes of vibrations. Furthermore, the first-order hyperpolarizabilities, total dipole moment, NBO and HOMO-LUMO energy gap have been calculated by using B3LYP methods with 6-31G (d, p) and 6-311G (d, p) basis sets in order to get an insight into the compound. The MEP map shows that the negative potential sites are on electronegative atoms while the positive potential sites are around the hydrogen atoms. The nonlinear optical properties revealed by theoretical calculations indicate that the studied compounds are good candidates of nonlinear optical materials.

References

[1] Y.X. Sun, Q.L. Hao, W.X. Wei, Z.X. Yu, L.D. Lu, X. Wang, Y.S. Wang, Experimental and density functional studies on 4-(3,4-dihydroxybenzylideneamino) antipyrine, and 4-(2,3,4-trihydroxybenzylideneamino)antipyrine, J. Mol. Struct. Theochem. 904 (2009) 74–82.
[2] C. Andraud, T. Brotin, C. Garcia, F. Pelle, P. Goldner, B. Bigot, A. Collet, Theoretical and experimental investigations of the nonlinear optical properties of vanillin, polyenovanillin, and bisvanillin derivatives, J. Am. Chem. Soc. 116 (1994) 2094–2102.
[3] M. Nakano, H. Fujita, M. Takahata, K. Yamaguchi, Theoretical study on second hyperpolarizabilities of phenylacetylene dendrimer: toward an understanding of structure-property relation in NLO responses of fractal antenna dendrimers, J. Am. Chem. Soc. 124 (2002) 9648–9655.
[4] V.M. Geskin, C. Lambert, J.L. Bredas, Origin of high second- and third-order nonlinear optical response in ammonio/boratodiphenylpolyene zwitterions: the remarkable role of polarized aromatic groups, J. Am. Chem. Soc. 125

(2003) 15651–15658.
[5] D. Sajan, H. Joe, V.S. Jayakumar, J. Zaleski, Structural and electronic contributions to hyperpolarizability in methyl p-hydroxy benzoate, J. Mol. Struct. 785 (2006) 43–53.
[6] Kanchana S. Thanthiriwatte, K.M. Nalin de Silva, Non-linear optical properties of novel fluorenyl derivatives—abinitio quantum chemical calculations, J. Mol. Struct. Theochem. 617 (2002) 169–175.
[7] N. Benhalima, K. Toubal, A. Chouaih, G. Chita, S. Maggi, A. Djafri, F. Hamzaoui, Synthesis and molecular structure investigation by DFT and x-ray diffraction of ARNO, J. Chem. Crystallogr. 41 (2011) 1729–1736.
[8] K. Toubal, A. Djafri, A. Chouaih, A. Talbi, Synthesis and structural determination of novel 5-Arylidene-3-*N*(2-alkyloxyaryl)-2- thioxothiazolidin- 4 -ones, Molecules 17 (2012) 3501–3509.
[9] A.D. Becke, Density functional thermochemistry. III. The role of exact exchange, J. Chem. Phys. 98 (1993) 5648.
[10] C. Lee, W. Yang, R.G. Parr, Development of the Colic-Salvetti correlation-energy formulainto a functional of the electron density, Phys. Rev. B37 (1988) 785.
[11] P. Hohenberg, W. Kohn, Homogeneous electron gas, Phys. Rev. 136 (1964) 864–B871.
[12] M.J. Frisch, G.W. Trucks, H.B. Schlegel, G.E. Scuseria, M.A. Robb, J.R. Cheeseman, J.A. Montgomery Jr., T. Vreven, K.N. Kudin, J.C. Burant, J.M. Millam, S.S. Iyengar, J. Tomasi, V. Barone, B. Mennucci, M. Cossi, G. Scalmani, N. Rega, G.A. Petersson, H. Nakatsuji, M. Hada, M. Ehara, K. Toyota, R. Fukuda, J. Hasegawa, M. Ishida, T. Nakajima, Y. Honda, O. Kitao, H. Nakai, M. Klene, X. Li, J.E. Knox, H.P. Hratchian, J.B. Cross, V. Bakken, C. Adamo, J. Jaramillo, R. Gomperts, R.E. Stratmann, O. Yazyev, A.J. Austin, R. Cammi, C. Pomelli, J.W. Ochterski, P.Y. Ayala, K. Morokuma, G.A. Voth, P. Salvador, J.J. Dannenberg, V.G. Zakrzewski, S. Dapprich, A.D. Daniels, M.C. Strain, O. Farkas, D.K. Malick, A.D. Rabuck, K. Raghavachari, J.B. Foresman, J.V. Ortiz, Q. Cui, A.G. Baboul, S. Clifford, J. Cioslowski, B.B. Stefanov, G. Liu, A. Liashenko, P. Piskorz, I. Komaromi, R.L. Martin, D.J. Fox, T. Keith, M.A. Al-Laham, C.Y. Peng, A. Nanayakkara, M. Challacombe, P.M.W. Gill, B. Johnson, W. Chen, M.W. Wong, C. Gonzalez, J.A. Pople, Gaussian 03, Revision C.02, Gaussian Inc., Wallingford, CT, 2004.
[13] M.H. Jamroz, Vibrational Energy Distribution Analysis: VEDA 4,Warasaw, Poland, 2004-2010.
[14] M.H. Jamróz, JCz. Dobrowolski, R. Brzozowski, Vibrational modes of 2.6 -2.7 and 2.3 – di isopropylnaphthalene. A DFT study, J. Mol. Struct. 787 (2006) 172–183.
[15] E.D. Glendening, A.E. Reed, J.E. Carpenter, F. Weinhold, NBO 3.0 Program Manual, Natural Bond Orbital/Natural Population Analysis/Natural Localized Molecular Orbital Programs, University of Wisconsin, Madison, 1998.
[16] R.N. Singh, Amit Kumar, P. Rawat, R.K. Tiwari, A.K. Singh, Studies on molecular structure, spectral analysis, chemical rea, J. Mol. Struct. 1052 (2013) 67–75.
[17] F. Furche, R. Ahlrichs, Adiabatic time-dependent density functional methods for excited state properties, J. Chem. Phys. 117 (2002) 7433–7447.
[18] G. Scalmani, M.J. Frisch, B. Mennucci, J. Tomasi, R. Cammi, V. Barone, Geometries and properties of excited states in the gas phase and in solution: theory and application of a time-dependent density functional theory polarizable continuum model, J. Chem. Phys. 124 (2006) 1–15.
[19] M.E. Casida, C. Jamorski, K.C. Casida, D.R. Salahub, Molecular excitation energies to high-lying bound states from time-dependent density-functional response theory: characterization and correction of the time-dependent local density approximation ionization threshold, J. Chem. Phys. 108 (1998) 4439–4449.
[20] J.L. Oudar, D.S. Chemla, J. Chem. Phys. 66 (1977) 2664.
[21] J.L. Oudar, J. Chem. Phys. 67 (1977) 446.
[22] H.A. Kurtz, J.J.P. Stewart, K.M. Dieter, Calculation of the nonlinear optical properties of molecules, J. Comput. Chem. 11 (1990) 82.
[23] G.J.B. Hurst, M. Dupuis, E. Clementi, J. Chem. Phys. 89 (1988) 385.
[24] Y. Atalay, D. Avcı, A. Basoglu, Linear and non-linear optical properties of some donor–acceptor oxadiazoles by ab initio Hartree-Fock calculations, Struct. Chem. 19 (2008) 239–246.
[25] M. Springborg, K. Schmidt, H. Meider, L.D. Marı0a, Theoretical studies of electronic properties of conjugated polymers, in: R. Farchioni, G. Grosso (Eds.), Organic Electronic Materials Conjugated Polymers and Low Molecular. Weight Organic Solids, Springer-Verlag Berlin Heidelberg, Germany, 2001.
[26] M. Arivazhagan, S. Jeyavijayan, Vibrational spectroscopic, first-order hyperpolarizability and HOMO, LUMO studies of 1,2-dichloro-4-nitrobenzene based on Hartree–Fock and DFT calculations, Spectrochim. Acta Part A 79 (2011) 376–383.
[27] M. Silverstein, G. Clayton Basseler, C. Morill, Spectrometric Identification of Organic Compounds, Wiley, New York, 1981.
[28] V. Krishna Kumar, S. Dheivamalar, R. John Xavier, V. Balachandran, Analysis of vibrational spectra of 4-amino-2,6-dichloropyridine and 2-chloro-3,5-dinitropyridine based on density functional theory calculations, Spectrochim. Acta A 65 (2006) 147–154.
[29] J.B. Lambert, H.F. Shurvell, L. Verbit, R.G. Cooks, G.H. Stout, Organic Structural Analysis, Macmillan Publ. Co. Inc., New York, 1976.
[30] G. Varsanyi, Vibrational Spectra of Benzene Derivatives, Academic Press, New York, 1969.
[31] M. Ramalingam, V. Sethuraman, N. Sundaraganesan, Molecular structure, vibrational spectroscopic, first order hyperpolarizability and HOMO–LUMO studies of 7-amino-8-oxo-3-vinyl-5-thia-1-azabicyclo[4.2.0]oct-2-ene-2-carboxylic acid, Spectrochim. Acta A78 (2011) 660–669.
[32] P.S. Kalsi, Spectroscopy of Organic Compounds, Academic Press, New York, 2002.
[33] G. Socrates, Infrared and Raman Characteristic Group Frequencies, Tables and Charts, third ed., Wiley, Chichester, 2001.
[34] L.J. Bellamy, The Infrared Spectra of Complex Molecules, third ed., Wiley, New York, 1975.
[35] N. Dege, N. Şenyüz, H. Batı, N. Günay, D. Avcı, Ö. Tamer, Y. Atalay, Spectrochim. Acta A 120 (2014) 323–331.
[36] D. Avcı, Y. Atalay, Effet of defferent GIAO and CSGT models and basis sets on 2-aryl-1,3,4-oxadiazole derivatives, J. Struct. Chem. 20 (2005) 185–201.
[37] N.B. Colthup, L.H. Daly, S.E. Wiberley, Introduction to Infrared and Raman Spectroscopy, Academic Press, New York, 1990.
[38] A. Suvitha, S. Periandy, S. Boomadevi, M. Govindarajan, Vibrational frequency analysis, FT-IR, FT-Raman, ab initio, HF and DFT studies, NBO, HOMO–LUMO and electronic structure calculations on pycolinaldehyde oxime, Spectrochim. Acta Part A Mol. Biomol. Spectrosc. 117 (2014) 216–224.
[39] G. Shakila, H. Saleem, N. Sundaraganesan, FT-IR, FT-Raman, NMR and U-V Spectral investigation: computation of vibrational frequency, chemical shifts and electronic structure calculations of 1-bromo-4-nitrobenzene, World Sci. News 61 (2017) 150–185.
[40] M. Snehalatha, C. Ravikumar, I. Hubert Joe, N. Sekar, V.S. Jayakumar, Spectroscopic analysis and DFT calculations of a food additive Carmoisine, Spectrochim. Acta Part A72 (2009) 654–662.
[41] M. Kaur, Y.S. Mary, H.T. Varghese, C.Y. Panicker, H.S. Yathirajan, M.S. Siddegowda, C.V. Alsenoy, Vibrational spectroscopic, molecular structure, first hyperpolarizability and NBO studies of 40-methylbiphenyl-2-carbonitrile, Spectrochim. Acta A 98 (2012) 91.
[42] D.W. Schwenke, D.G. Truhlar, Systematic study of basis set superposition errors in the calculated interaction energy of two HF molecules, J. Chem. Phys. 82 (1985) 2418–2426.
[43] A. Esme, S.G. Sagdinc, The vibrational studies and theoretical investigation of structure, electronic and non-linear optical properties of Sudan III [1-{[4-(phenylazo) phenyl]azo}-2-naphthalenol], J. Mol. Struct. 1048 (2013) 185–195.
[44] R.S. Mulliken, Electronic population analysis on LCAOMO molecular wave function, J. Chem. Phys. 23 (1955) 1833–1840.
[45] A.E. Reed, L.A. Curtiss, F. Weinhold, Intermolecular interactions from a naturel bond orbital, donor-acceptor viewpoint, Chem. Rev. 88 (1988) 899–926.
[46] C. Andraud, T. Brotin, F.Pelle Garcia, P. Goldner, B. Bigot, A. Collet, Theoretical and experimental investigations of the nonlinear optical properties of vanillin, polyenovanillin, and bisvanillin derivatives, J. Am. Chem. Soc. 116 (1994) 2094–2102.
[47] V.M. Geskin, C. Lambert, J.L. Bredas, Origin of high second- and third-order nonlinear optical response in ammonio/borato diphenylpolyene zwitterions: the remarkable role of polarized aromatic groups, J. Am. Chem. Soc. 125 (2003) 15651–15658.
[48] M. Nalano, H. Fujita, M. Takahata, K. Yamaguchi, Theoretical study on second hyperpolarizabilities of phenylacetylene dendrimer: toward an understanding of structure– property relation in nlo responses of fractal antenna dendrimers, J. Am. Chem. Soc. 124 (2002) 9648–9655.
[49] D. Sajan, I.H. Joe, V.S. Jayakumar, J. Zaleski, Structural and electronic contributions to hyperpolarizability in methyl p-hydroxy benzoate, J. Mol. Struct. 785 (2006) 43–53.
[50] D.A. Kleinman, Phys. Rev. 126 (1962) 1977–1979.
[51] R. Zhang, B. Du, G. Sun, Y. Sun, Spectrochim. Acta Part A Mol. Biomol. Spectrosc. 75 (2010) 1115–1124.
[52] E. Gobinath, R.J. Xavier, Quantum chemical calculations, vibrational studies, HOMO–LUMO and NBO/NLMO analysis of 2-bromo-5-nitrothiazole, Spectrochim. Acta Part A Mol. Biomol. Spectrosc. 104 (2013) 394–402.
[53] S. Alturk, N. Boukabcha, N. Benhalima, O. Tamer, A. Chouaih, D. Avcı, Y.Atalay, F. Hamzaoui, Conformational, spectroscopic and nonlinear optical investigations on 1-(4-chlorophenyl)-3-(4-chlorophenyl)-2-propen-1-one: a DFT study, Indian J. Phys. 91 (2017) 501–511.
[54] S. Chand, F.A.M. Al-Omary, A.A. El-Emam, V.K. Shukla, O. Prasad, L. Sinha, Study on molecular structure, spectroscopic behavior, NBO, and NLO analysis of 3-methylbezothiazole-2-thione, Spectrochim. Acta Part A Mol. Biomol. Spectrosc. 146 (2015) 129–141.
[55] I. Fleming, Frontier Orbitals, Organic Chemical Reactions, Wiley, London, 1976.
[56] B. Kosar, C. Albayrak, Spectroscopic investigations and quantum chemical

computational study of (*E*)-4-methoxy-2-[(p-tolylimino)methyl]phenol, Spectrochim. Acta A 78 (2011) 160–167.
[58] Z. Demircioğlu, Ç. Albayrak, O. Büyükgüngör, Experimental (X-ray, FT-IR and UV–vis spectra) and Theoretical Methods (DFT study) of (E)-3-methoxy-2-[(ptolylimino) methyl]phenol, Spectrochim. Acta Part A Mol. Biomol. Spectrosc. 128 (2014) 748–758.
[59] R. Mishra, A. Srivastava, A. Sharma, P. Tandon, C. Baraldi, M.C. Gamberini, Spectrochim. Acta Part A Mol. Biomol. Spectrosc. 101 (2013) 335–342.